Sparse Coding and Decorrelation in Primary Visual Cortex During Natural Vision

William E. Vinje[1,2] and Jack L. Gallant[1,3]*

Theoretical studies suggest that primary visual cortex (area V1) uses a sparse code to efficiently represent natural scenes. This issue was investigated by recording from V1 neurons in awake behaving macaques during both free viewing of natural scenes and conditions simulating natural vision. Stimulation of the nonclassical receptive field increases the selectivity and sparseness of individual V1 neurons, increases the sparseness of the population response distribution, and strongly decorrelates the responses of neuron pairs. These effects are due to both excitatory and suppressive modulation of the classical receptive field by the nonclassical receptive field and do not depend critically on the spatiotemporal structure of the stimuli. During natural vision, the classical and nonclassical receptive fields function together to form a sparse representation of the visual world. This sparse code may be computationally efficient for both early vision and higher visual processing.

Although area V1 has been studied for over 40 years, little is known about how V1 encodes complex natural scenes. Theoretical studies suggest that natural scenes can be efficiently represented by a sparse code based on filters that resemble neurons found in area V1 (*1, 2*). Sparse codes lie along a continuum ranging from dense codes, where neurons respond to most stimuli, to local codes, where neurons give extremely selective responses (*3*). Both of these extremes are inefficient in several important respects. Dense codes are highly redundant and each neural response carries little information, whereas local codes require an implausibly large number of neurons and are computationally intractable. In contrast, neurons that are tuned to match the sparsely distributed, informative components of the natural world can produce sparse codes. Sparse codes transmit information with minimal redundancy and relatively few spikes. Consequently, they are both informationally and metabolically more efficient than dense codes (*4*). There have been a few studies of sparse coding in inferior temporal visual areas (*5*). We have addressed this issue in area V1.

Recent theoretical studies suggest that nonlinear interactions between neurons may increase coding sparseness in area V1 (*2, 6*). These interactions are predominantly reflected in modulation of classical receptive field (CRF) responses by the surrounding nonclassical receptive field (nCRF) (*7*). Previous experiments have demonstrated that nCRF stimulation strongly modulates responses during free viewing of natural scenes (*8*). This report demonstrates that V1 employs a sparse code to represent natural scenes and shows that the nCRF plays a crucial role in this process.

We have addressed this issue by using controlled stimuli that simulate natural vision. The stimuli were sequences of images simulating the spatial and temporal patterns occurring in and around the CRF when an animal freely views a static natural scene (see Fig. 1A). Eye scan paths were generated with a statistical model of eye movements made during free viewing (*9*). Image patches were extracted from a natural scene along the simulated scan path and converted to gray scale (*10*). Each natural vision movie was composed of a series of simulated fixations separated by brief simulated saccadic transitions.

In the experiments described here, we manipulated the size of the extracted image patches. Patch size varied from one to four times the diameter of the CRF. To reduce potential boundary artifacts, the outer 10% of each image patch was blended smoothly into the neutral gray background. Data reported here are from 61 well-isolated neurons recorded in area V1 of two awake behaving primates (*11*).

The sparseness of V1 responses increases dramatically with larger natural image patches that encompass both the CRF and the nCRF. This effect is illustrated in Fig. 1, which compares responses obtained with stimuli confined to the CRF (Fig. 1B) with those obtained with stimuli four times the diameter of the CRF (Fig. 1C). To quantify sparseness we used a nonparametric statistic (*12*): $S = \{1 - [(\Sigma r_i/n)^2/\Sigma(r_i^2/n)]\}/[1 - (1/n)]$, where r_i is the response to the ith frame of a movie (averaged across trials) and n is the number of movie frames. Values of S near 0% indicate a dense code, and values near 100% indicate a sparse code.

Distributions of S across the sample of neurons are shown in Fig. 2 for each stimulus size. As stimulus size increases, sparseness increases systematically ($P < 0.01$) (*13*). The sparseness statistic saturates when stimuli are three to four times the size of the CRF, consistent with the spatial extent of V1 nCRF modulation reported in other studies (*7*). The high sparseness values produced by large stimuli suggest that area V1 uses a sparse code during natural vision, when stimuli span the entire visual field.

The simulated saccades in our natural vision movies often produce large transient responses followed by rapid adaptation during the course of the fixation. To assess the contribution of this fine temporal structure to sparseness, we recomputed the sparseness statistic after averaging all responses within each fixation. Absolute sparseness values are significantly lower in the fixation-based analysis ($P < 0.05$), but sparseness still increases with increasing nCRF stimulation (*14*). Thus, transient responses and adaptation contribute to sparseness but do not account for all of the observed nCRF effects.

We reanalyzed a subset of cells to determine whether these sparsening effects were due to nCRF suppression, excitation, or both ($n = 36$ cells; stimuli four times the CRF diameter). Twenty-nine percent of all the frames in this sample are significantly modulated ($P < 0.05$), and the ratio of suppression to excitation is about 4.5 to 1. Excitation is often concentrated in the onset transients that occur after simulated saccades, whereas suppression reduces responses across an entire fixation. Thus, natural nCRF stimulation appears to increase sparseness by both enhancing and suppressing specific epochs of the response.

It is unlikely that these results are an artifact of incorrect CRF definition (*15*). We defined the CRF as the circular region circumscribing all locations where stimuli evoked action potentials. Overestimation of CRF sizes would cause inadvertent nCRF stimulation by movies confined to the nominal CRF, thereby increasing estimates of CRF sparseness and decreasing the apparent sparsening effects of nCRF stimulation.

We also performed a control experiment to ensure that our sparseness estimates did not depend on the position of the patch boundary, which necessarily varied with patch size. The control stimulus consisted of a natural vision movie four times the CRF diameter on which a sharp, white ring was superimposed along the exterior boundary of the defined CRF. The ring provided a strong artificial edge to enhance the magnitude of

[1]Program in Neuroscience, [2]Department of Molecular and Cellular Biology, and [3]Department of Psychology, University of California at Berkeley, Berkeley, CA 94720–1650, USA.

*To whom correspondence should be addressed. E-mail: gallant@socrates.berkeley.edu

any potential edge effects. Ring trials were randomly interleaved with non-ring trials. The addition of the CRF-diameter ring increases sparseness by an average of 8% (n = 12 neurons) relative to that observed without the ring. Thus, sparseness estimates for CRF-diameter stimuli may be inflated slightly because of the presence of the sharp border, which suggests that our estimates of the sparsening effects of nCRF stimulation probably underestimate the true size of this effect.

The data presented above were acquired with controlled stimuli that simulate natural vision. During natural free viewing, V1 activity reflects both visual stimulation and modulation by extraretinal factors such as eye movements and attention (*16*). We examined how these extraretinal factors affect sparseness by comparing responses obtained during free viewing of natural scenes (*17*) to responses obtained with natural vision movies that re-created the visual stimulation occurring in the CRF and the surround during the same free-viewing episodes (*18*). Both free-viewing and natural vision movie data were acquired in 11 V1 neurons (17 separate free-viewing episodes). Sparseness values obtained during free viewing and with natural vision movies are highly correlated (r = 0.91). However, the slope of the regression line is 1.2, which suggests that free viewing produces a slightly more sparse response than do natural vision movies simulating free viewing. Given that the movies may not fully stimulate the nCRF of some cells, this small difference is expected, but we cannot rule out the possibility of weak extraretinal effects.

As a final control, we examined sparseness values obtained with dynamic grating sequences (n = 22 neurons) (*19*) to see if sparsening is specific to natural stimuli. To compare response sparseness for random grating sequences and natural vision movies, we computed S for both stimulus types and for stimuli one and two times the size of the CRF. The sparseness values obtained with gratings and natural vision movies are not significantly different from each other, which suggests that sparseness might be induced by oriented energy present in both natural stimuli and grating sequences.

The sparse coding hypothesis also predicts that responses will be sparse when examined across the population of neurons in V1. To investigate this, we evaluated the kurtosis of the response distribution (RD) obtained with each stimulus size. The RD is the histogram of responses (i.e., action potentials per movie frame) pooled over all cells and all stimuli; it is an estimate of the population response of V1 to an ensemble of

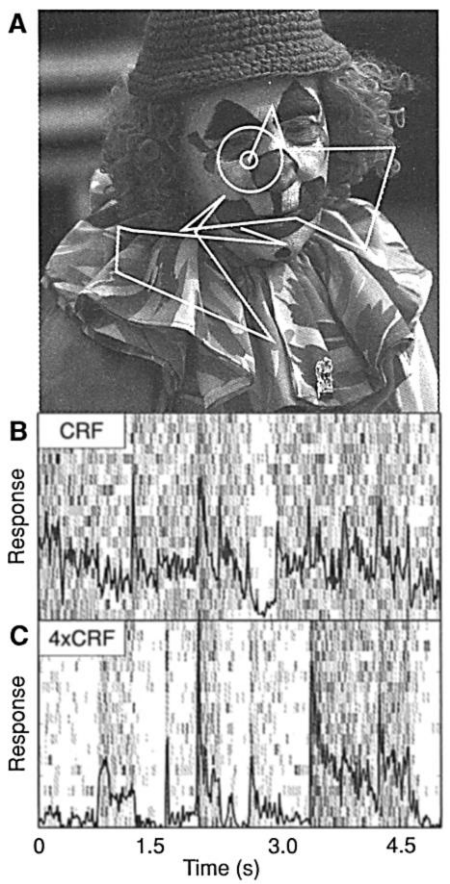

Fig. 1. Natural vision movie and representative responses. **(A)** Example of a natural scene used as the source image for natural vision movies. White line represents simulated visual scan path. Image patches centered on the scan path were extracted to form the movie. Small white circle gives the CRF size; larger circle is four times the CRF diameter. **(B)** Raster plot of action potentials during 20 presentations of a movie confined to the CRF. The number of action potentials during each 13.8-ms movie frame is indicated by intensity. Solid line is the peri-stimulus time histogram (PSTH). The sparseness of these data is 16%, which implies a dense distribution of responses across the stimulus set. **(C)** Raster plot of action potentials during 20 presentations of a movie with a stimulus size four times the CRF diameter. Dark line again gives the PSTH. Stimulation of the nCRF increases sparseness to 53%.

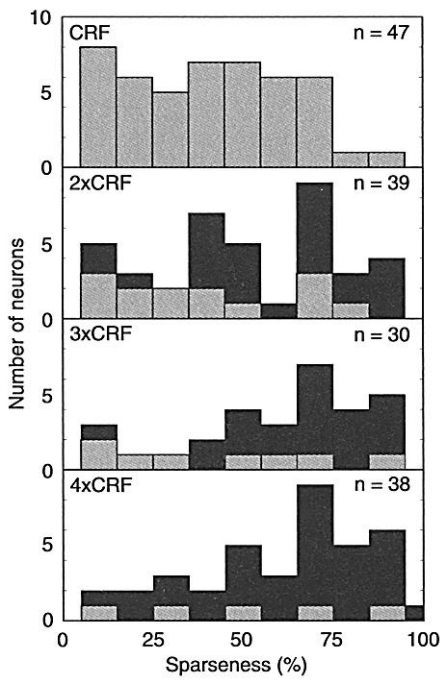

Fig. 2. Stimulation of the nCRF increases sparseness in single neurons. Effects of stimulus size on distribution of the sparseness statistic across the sample of cells. Expressed as a percentage, S is 0% when a neuron responds equally to all frames of a movie and 100% when a neuron responds to only a single frame. An increase in S indicates an increase in the sparseness of neural coding across the stimulus ensemble. Mean sparseness values are 41%, 52%, 61%, and 62% for stimuli one, two, three, and four times the CRF diameter, respectively. To quantify sparseness changes in single neurons we computed the ratio of the observed shift in S to the maximum possible shift as a function of nCRF stimulation: $S_{shift} = (S_{nCRF} - S_{CRF})/(1 - S_{CRF})$. Average S_{shift} values are 18%, 32%, and 36% for stimuli two, three, and four times the CRF diameter, respectively. Neurons with statistically significant ($P < 0.01$) shifts are black and are stacked on top of those with insignificant shifts.

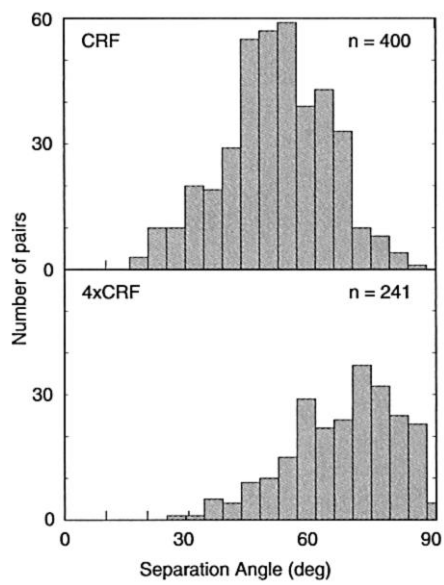

Fig. 3. Stimulation of the nCRF decorrelates responses across the population of neurons in area V1. **(Upper)** Distribution of upper limits of the separation angles between pairs of neurons tested with similar natural vision movies confined to the CRF. Separation angle is inversely proportional to the similarity of responses between randomly selected V1 neurons recorded in separate sessions [see text and (*21*) for details]. The mean separation angle is 51°, indicating substantial response similarity. **(Lower)** Distribution of upper limits of the separation angles between neuron pairs obtained with natural vision movies four times the CRF diameter, plotted as in (Upper). The mean of this distribution is 67°, which is significantly larger than the mean of the distribution obtained from CRF stimulation alone ($P \leq 0.001$). This increase in separation angle reflects decorrelation across the population of V1 responses.

natural images. Kurtosis is the fourth moment of this distribution about its mean value. As the RD becomes more sparse the proportion of moderate responses decreases and the proportion of both small and large responses increases; this is reflected by an increase in RD kurtosis. For this reason, theorists have used kurtosis as an index of sparseness (*2, 20, 21*).

RD kurtosis is 4.1 when stimuli are confined to the CRF, consistent with theoretical studies suggesting that the CRF of V1 neurons produces a moderately sparse code (*1*). However, when stimuli are two, three, or four times the CRF diameter, kurtosis values increase significantly to 5.2, 8.7, and 10.2, respectively ($P \leq 0.001$). This result further confirms that nonlinear nCRF interactions increase sparseness and demonstrates that this effect occurs across the population of cells in V1.

We also tested whether nCRF stimulation increased the independence of responses across the population of V1 neurons. We accomplished this by examining the similarity of responses between randomly selected pairs of neurons presented with nearly identical stimuli during different recording sessions. This similarity reflects the distribution of correlations across the entire population of cells in V1. If neurons carry independent information, then randomly selected pairs will be weakly correlated, whereas if they carry redundant information responses will be strongly correlated.

We selected neuron pairs stimulated with natural vision movies created from the same eye scan path and natural scene (patch sizes varied slightly because of differences in CRF size). For this analysis the average responses across movie frames were treated as a vector in a high-dimensional space. We quantified response similarity by computing the angle between the response vectors of each neuron pair (*22*). Using this metric, cells with similar tuning properties have small separation angles and those with different tuning properties have large separation angles.

Figure 3 shows the distribution of separation angles between neuron pairs recorded with natural vision movies confined to the CRF (Fig. 3, Upper) and four times larger than the CRF (Fig. 3, Lower). Stimulation of the nCRF significantly increases the separation angle between cells ($P \leq 0.001$) (*23*). This is direct evidence that nCRF stimulation decorrelates responses between pairs of V1 neurons and it suggests that one consequence of increasing sparseness is increased independence of the responses across cells.

In a final experiment we investigated the nCRF mechanisms that might be responsible for sparsening and decorrelation. We accomplished this by mapping the spatial domains of the nCRF via reverse correlation. The stimulus was a dynamic, compound grating sequence consisting of a CRF conditioning grating and an nCRF probe extending to two times the CRF size [see Fig. 4A and (*24*)]. The strength, sign, and spatial distribution of nCRF domains vary widely across cells (n = 19 neurons) (see Fig. 4, B to D). Many cells have irregular nCRF domains (Fig. 4, B and C), although some have a fairly uniform structure (Fig. 4D). These patterns are similar to those reported recently for area 17 of the anesthetized cat (*25*). The diversity of the nCRF structure may be responsible for decorrelating the responses of V1 neurons during natural vision.

Our experiments provide direct experimental evidence that V1 uses a sparse code matched to the underlying sparse structure of natural scenes. During natural vision, CRF and nCRF mechanisms function together as a single computational unit. Although CRF responses during natural vision are already moderately sparse, nCRF stimulation elicits nonlinear interactions (*2, 6*) that dramatically increase sparseness and decorrelate responses between neurons. Consequently, each neuron appears to carry statistically independent information. Between the retina and lateral geniculate nucleus, the visual system encodes information to optimize information transmission given the limited bandwidth of the optic nerve (*26*). V1 then recodes this information into a sparse representation. One interesting possibility is that these cells represent the independent components of natural scenes (*20, 27*). This would facilitate the development of associations between visual stimuli in higher visual areas and increase the efficiency of pattern recognition (*1*).

Sparse coding provides a unifying framework for understanding the diverse functions claimed for the nCRF: such as contrast gain control; the potential representation of extended contours, junctions or corners; and figure-ground segmentation (*28*). Our studies demonstrate how experiments with natural images can complement those with conventional stimuli. When used carefully, natural stimuli allow us to test our current understanding of sensory systems and to interpret known effects in terms of their natural function.

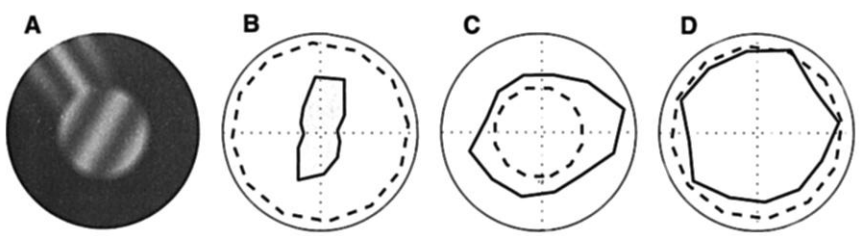

Fig. 4. Identification of nCRF subdomains by reverse correlation. **(A)** Example of a single frame from the compound grating sequence. An optimal conditioning grating filled the CRF while a probe grating appeared in the annulus between the CRF and twice the CRF diameter. Probe position, orientation, spatial frequency, and phase varied randomly across frames (*24*). Spatial modulatory nCRF domains were identified by reverse correlation with respect to the position of the probe within the nCRF. **(B)** Anisotropic inhibitory nCRF modulation. Solid curves indicate mean response as a function of probe position. Dashed lines give mean responses to the conditioning grating alone. Plots are rotated so the preferred orientation of the CRF lies along the vertical axis. This cell is suppressed by nCRF stimulation; side suppression is larger than end suppression. **(C)** A cell that is enhanced by nCRF stimulation; side enhancement is larger than end enhancement. **(D)** A cell that is weakly and uniformly suppressed by nCRF stimulation. For all three neurons shown here, nCRF stimulation with natural vision movies significantly increases sparseness ($P < 0.01$).

References and Notes

1. H. B. Barlow, in *Sensory Communication*, W. A. Rosenblith, Ed. (MIT Press, Cambridge, MA, 1961), pp. 217–234; *Neural Comput.* **1**, 295 (1989); J. G. Daugman, *IEEE Trans. Biomed. Eng.* **36**, 107 (1989); D. J. Field, *J. Opt. Soc. Am. A* **4**, 2379 (1987); *Neural Comput.* **6**, 559 (1994).
2. B. A. Olshausen and D. J. Field, *Nature* **381**, 607 (1996); *Vision Res.* **23**, 3311 (1997).
3. P. Foldiak and M. P. Young, in *The Handbook of Brain Theory and Neural Networks*, M. A. Arbib, Ed. (MIT Press, Cambridge, MA, 1995), pp. 895–898.
4. W. Levy and R. A. Baxter, *Neural Comput.* **8**, 531 (1996); S. B. Laughlin, R. R. de Ruyter van Steveninck, J. C. Anderson, *Nat. Neurosci.* **1**, 36 (1998).
5. M. P. Young and S. Yamane, *Science* **256**, 1327 (1992); E. T. Rolls and M. J. Tovee, *J. Neurophysiol.* **73**, 713 (1995); R. Baddeley *et al., Proc. R. Soc. London Ser. B* **264**, 1775 (1997).
6. E. P. Simoncelli and O. Schwartz, in *Advances in Neural Information Processing Systems 11*, M. I. Jordan, M. J. Kearns, S. A. Solla, Eds. (MIT Press, Cambridge, MA, 1998).
7. J. Allman, F. Miezin, E. McGuinness, *Annu. Rev. Neurosci.* **8**, 407 (1985) pp. 153–154.
8. J. L. Gallant, C. E. Connor, D. C. Van Essen, *Neuroreport* **9**, 2153 (1998).
9. We generated saccadic eye scan paths by using a model of natural macaque eye movements. We acquired eye movement data from a scleral search coil during free-viewing experiments (*8, 17*). The model chose random saccade directions from a uniform distribution of angles. We chose saccade lengths randomly from a distribution based on a b-spline fit to the measured distribution of free-viewing saccade lengths. The eye velocity versus time profile for each saccade was obtained from a lookup table of b-spline fits to actual velocity/time profiles (as a function of saccade length). We chose fixation durations from a gaussian distribution (mean, 350 ms; standard deviation, 50 ms).
10. We extracted image patches from 1280 × 1024 pixel images obtained from a high-resolution, commercial photo-CD library (Corel Inc.). Images included nature scenes as well as man-made objects and animals as well as humans. To avoid aliasing artifacts that might result from displaying movies on a monitor with

72-Hz refresh we used an antialiasing algorithm in which each 13.8-ms frame of a movie was constructed by averaging 14 images representing the position of the CRF at about 1-ms resolution.

11. All animal procedures were approved by the University of California, Berkeley, Animal Care and Use Committee and conformed to or exceeded all relevant National Institutes of Health and U.S. Department of Agriculture standards. Single neuron recordings were made from two awake, behaving macaque monkeys (*Macaca mulatta*) with extracellular electrodes. Additional details about recording and surgical procedures are given in [C. E. Connor *et al.*, *J. Neurosci.* **17**, 3201 (1997)]. All data reported here were taken under conditions of excellent single-unit isolation. Eye position was monitored with a scleral search coil and trials were aborted if the eye deviated from fixation by more than 0.35°. Movie duration varied from 5 to 10 s. During recording sessions each movie was divided into 5-s segments; segments were then shown in and around the CRF on successive trials while the animal performed a fixation task for a juice reward. Each trial consisted of a stimulus of a single size with differently sized stimulus conditions randomly interleaved across trials.
12. A well-established and useful description of how sparsely a neuron responds across stimuli is given by its activity fraction, $A = (\Sigma r_i/n)^2/\Sigma(r_i^2/n)$. For further discussion see [E. T. Rolls and M. J. Tovee, *J. Neurophysiol.* **73**, 713 (1995)]. Our sparseness statistic is a convenient rescaling of A that ranges from 0% to 100%: $S = (1 - A)/(1 - A_{MIN}) = (1 - A)/(1 - 1/n)$.
13. Throughout this report we measured significance with randomization tests using 1000 random permutations of the relevant data. For further discussion see [B. F. J. Manly, *Randomization and Monte-Carlo Methods in Biology*, (Chapman & Hall, New York, 1991)].
14. If responses are averaged within a fixation, sparseness declines from 41 to 23%, 52 to 34%, 61 to 42%, and 62 to 45% for stimuli one, two, three, and four times the size of the CRF, respectively.
15. The boundaries of the CRF were estimated with bar and grating stimuli whose characteristics were controlled interactively. For 38 of 61 neurons we confirmed these manual estimates by reverse correlation on responses evoked by a dynamic sequence of small white squares distributed in and around the CRF (square positions were chosen randomly for each frame). Reliable CRF estimates were obtained with 150 to 300 s of data (30 to 60 behavioral fixation trials). Generally there is excellent agreement between the CRF profile estimates obtained with the two methods. Our CRF estimates ranged from about 20 to 50 min of arc, which is entirely consistent with the range of receptive field diameters obtained in awake behaving macaques by other researchers; for example, see [D. M. Snodderly and M. Gur, *J. Neurophysiol.* **74**, 2100 (1995)].
16. S. J. Judge, R. H. Wurtz, B. J. Richmond, *J. Neurophysiol.* **43**, 1133 (1980); B. C. Motter, *J. Neurophysiol.* **70**, 909 (1993).
17. Animals viewed high-resolution natural images digitized on commercial photo-CDs (Corel Corp.) and shown at a resolution of 1280 × 1024 pixels. Images were shown for 10 s each. Neural responses and eye position were recorded continuously during this free viewing (*8*). Natural vision movies that simulated these specific free-viewing episodes were constructed by using the eye position records to determine the position of the recorded CRF during free viewing. In six cells the diameter of the reconstructed movies was four times the CRF, and in 11 cells it was three times the CRF. These data have been combined in this report.
18. Each free-viewing episode produced a single-spike train evoked by a unique pattern of exploratory eye movements. In contrast, natural vision movies were repeated many times. To obtain comparable sparseness estimates for these data, we separately analyzed the spike train evoked by each repetition of the natural vision movie. The average of this distribution of sparseness values was then compared with the single sparseness value obtained from the free-viewing data. To ensure matched stimulus conditions, we made all comparisons on a movie-by-movie basis. Note that sparseness values based on single-spike trains are biased upward because of the discrete nature of spike generation.
19. The random sinusoidal grating sequence was similar to that used by D. L. Ringach, M. J. Hawken, R. Shapley [*Nature* **387**, 281 (1997)]. The orientation, spatial frequency, and phase of the grating were chosen randomly on each video frame (at 72 Hz). Gratings were shown at a Michelson contrast of 0.5. Before analysis, stimuli were binned into 10° orientation steps and 6 to 12 spatial frequency steps. Responses were analyzed by parametric reverse correlation on orientation and spatial frequency, averaging over phase. The mean responses across stimulus bins (at the peak response latency) were used to estimate the sparseness statistic.
20. A. J. Bell and T. J. Sejnowski, *Vision Res.* **37**, 3327 (1997).
21. Several theoretical studies of sparse population coding have reported the kurtosis of the distribution of responses observed across a set of linear filters, with respect to a particular stimulus ensemble (*2, 20*). This measure is not directly applicable to our data because the responses of area V1 neurons are asymmetric: cells typically exhibit low spontaneous rates and appropriate stimuli elevate these rates. To estimate kurtosis we converted each response distribution to a symmetric distribution by reflecting the data about the origin. The resulting symmetric distributions are unimodal with zero mean and decrease smoothly to zero. Our kurtosis statistic is well behaved and directly comparable to the results of theoretical studies.
22. Let P_1 and P_2 be the PSTH response vectors for a pair of neurons. Then $\cos(\theta) = P_1P_2/\|P_1\| \times \|P_2\|$, where $\|P_n\|$ is the norm of the appropriate vector. This measure is sensitive to changes across the basis dimensions of the movie time stream and is insensitive to differences in absolute rate.
23. It is difficult to choose a scalar measure of response similarity appropriate for all situations; see [P. Di Lorenzo, *J. Neurophysiol.* **62**, 823 (1989)]. To validate our results we performed two alternative versions of the population decorrelation analysis. For each neuron pair we also computed both the linear correlation coefficient and the neural discrimination index of Di Lorenzo. In both cases, nCRF stimulation leads to significant decorrelation ($P \leq 0.001$). To ensure that the slightly different stimulus sizes do not influence our results, we also performed all similarity analyses on a data set restricted to neuron pairs with identical CRF sizes (and thus identical stimulation). Under these conditions the decorrelating effect of the nCRF remains significant ($P \leq 0.001$).
24. The compound grating stimulus consisted of a CRF conditioning grating and a probe grating. We set the conditioning grating's orientation and spatial frequency to the neuron's preferred values [as determined by reverse correlation on responses to a dynamic grating sequence (*19*) presented in the CRF]. The phase of the conditioning grating varied randomly with each video frame. Both gratings were presented at a Michelson contrast of 0.5 and their edges were blended into one another and into the background. We performed reverse correlation on the position of the probe grating within the nCRF annulus (collapsing over all other parameters). To measure baseline responses we presented interleaved trials containing only the conditioning grating.
25. G. A. Walker *et al.*, *J. Neurosci.* **19**, 10536 (1999).
26. Y. Dan, J. J. Atick, R. C. Reid, *J. Neurosci.* **16**, 3351 (1996).
27. M. S. Lewicki and B. A. Olshausen, in *Advances in Neural Information Processing Systems 10*, M. I. Jordan, M. J. Kearns, S. A. Solla, Eds. (MIT Press, Cambridge, MA, 1997) pp. 815–821.
28. D. J. Heeger, *Visual Neurosci.* **9**, 181 (1992); C. D. Gilbert, *Neuron* **9**, 1 (1992); A. M. Sillito *et al.*, *Nature* **378**, 492 (1995); C. D. Gilbert *et al.*, *Proc. Natl. Acad. Sci. U.S.A.* **93**, 615 (1996); M. Carandini *et al.*, *J. Neurosci.* **17**, 8621 (1997); J. J. Knierim and D. C. Van Essen, *J. Neurophysiol.* **67**, 961 (1992).

20 August 1999; accepted 27 December 1999

Mitochondrial FtsZ in a Chromophyte Alga

Peter L. Beech,[1,3]* Thao Nheu,[3]† Thomas Schultz,[3]‡ Shane Herbert,[1] Trevor Lithgow,[4] Paul R. Gilson,[2,3] Geoffrey I. McFadden[2,3]

A homolog of the bacterial cell division gene *ftsZ* was isolated from the alga *Mallomonas splendens*. The nuclear-encoded protein (MsFtsZ-mt) was closely related to FtsZs of the α-proteobacteria, possessed a mitochondrial targeting signal, and localized in a pattern consistent with a role in mitochondrial division. Although FtsZs are known to act in the division of chloroplasts, MsFtsZ-mt appears to be a mitochondrial FtsZ and may represent a mitochondrial division protein.

Mitochondria are ubiquitous organelles that form networks, reticulae, or punctate structures in eukaryotic cells. Mitochondria in many cells appear to constitutively fuse with one another and divide (*1*), but we know little about the proteins involved in these processes, particularly mitochondrial division. Eukaryotes depend on mitochondria for respiration and adenosine triphosphate synthesis and rely on them to divide before daughter mitochondria can be apportioned to each new cell generation. In chloroplasts, homologs of the bacterial cell division protein FtsZ are essential components of the organellar division machinery (*2*). FtsZ is found in nearly all prokaryotes, is structurally related to tubulin, and accumulates at the furrow between dividing cells, playing a critical role in cell division (*3*). No potential mitochondrial FtsZ has been identified in the complete genomes of *Caenorhabditis elegans* or *Saccharomyces cerevisiae*. However, because both mitochondria and chloroplasts arose from endosymbiotic bacteria, we anticipated that early in evolution, mitochondrial division might also have been regulated by FtsZ. Here we de-